PCCP

Accepted Manuscript

ROYAL SOCIETY OF CHEMISTRY

www.rsc.org/pccp

Graphical Abstract

Three donor-acceptor organic conjugated small-molecules **BCz-BT**, **BCz-NO2** and **BCz-CN** with different electronic effect of the terminal acceptors were designed and synthesized and their application in memory devices with a sandwich configuration. The device based on the molecule with weak electronic effect between donor and acceptor (**BCz-BT**) induced volatile memory SRAM behaviour, ii) strong inductive effect but weak conjugative effect (**BCz-NO2**) induced non-volatile WORM characteristic, iii) strong inductive effect and conjugative effect (**BCz-BT**) caused non-volatile flash switch behaviour which arises from the formation of CT complex.

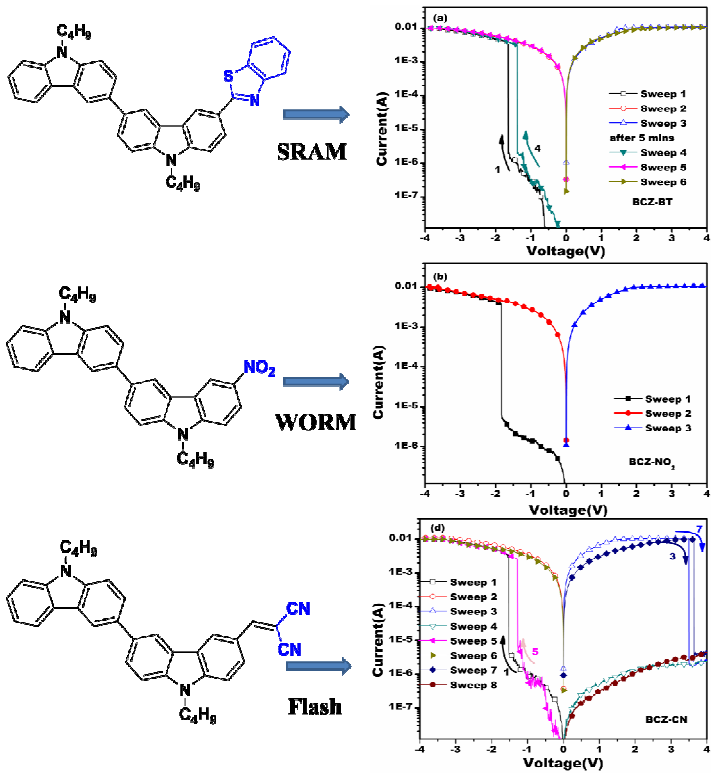

Cite this: DOI: 10.1039/c0xx00000x

www.rsc.org/xxxxxx

ARTICLE TYPE

Electronic Effect of Terminal Acceptor Groups on Organic Donor-Acceptor Small-Molecule Induced Different Memory Models

Haifeng Liu,[a] Hao Zhuang,[a] Hua Li,*[a] Jianmei Lu*[a,b] and Lihua Wang[a]

Received (in XXX, XXX) Xth XXXXXXXXX 20XX, Accepted Xth XXXXXXXXX 20XX

DOI: 10.1039/b000000x

In this work, three new donor-acceptor organic small-molecules, bicarbazole served as electron donor, benzothiazole, nitryl and 1, 1'-dicyanovinyl used as electron acceptor, were designed and synthesized to fabricate as sandwiched memory devices. Acceptors varying in electron-delocalized extent and electron-withdrawing strength were attached to the molecular backbone to investigate the effect of devices switching behaviors. The bi-n-butyl-carbazole-benzothiazole (**BCz-BT**) based memory device exhibited volatile static random access memory (SRAM) switching behaviour, bi-n-butyl-carbazole-nitryl (**BCz-NO_2**) was found to exhibit stable nonvolatile write-once-read-many-times (WORM) data storage characteristic and bi-n-butyl-carbazole-dicyanovinyl (**BCz-CN**) showed rewritable flash memory with a higher ON/OFF current ratio about 10^4. Therefore, tunable data storage devices through adjusting the terminal acceptor groups offer the feasible guidance for the rational design of organic molecules to achieve superior memory performance.

Introduction

Resistive memory devices based on organic materials with bistable conductance switching were investigated intensively in recent years because of the outstanding advantages of low cost potential, adjustable molecular structure and good processability and potentially application for the next generation memory devices[1-8]. Including random polymers[9-12], conjugated polymers[13-15] and organic small-molecules[16-20] etc. have been employed as resistive switching materials and achieved nonvolatile write-once-read-many-times (WORM), reversible flash memory, volatile dynamic random access memory (DRAM) and static random access memory (SRAM). To date, the researchers devoted numerous efforts to define the relationships between the molecular framework and the switch performances[21-23]. In particular, designed and synthesized the compounds based on donor-acceptor (D-A) model have attracted extensive attention because the donor-acceptor system facilitate: (i) charge-transfer (CT) complex formation under the effect of an external electric field and realize the device transformation from off state to on state; (ii) decrease of the carrier injection barrier (increase of the LUMO level and decrease of the HOMO level simultaneously); (iii) charge carrier transport in the solid state[24-27]. However, the electronic effect of interrelation between the electron-donating group and electron-withdrawing group on the switch behaviors is still necessary for a further study.

In order to deeper understanding the relationship between the interaction of the push-pull configuration and the memory properties, three donor-acceptor conjugated organic small-molecules with different terminal electron-withdrawing groups were synthesized and explored (Fig. 1c), (i) the benzothiazole unit shows weak negative electron effect and the π-electron could delocalize over a large area[28]; (ii) the nitryl is an intense electron withdrawing group, but the delocalized extent of π-electron is confined to the nitryl group around[29,30]; (iii) dicyanovinyl segment also plays a strong electron affinity role, but the delocalized extent of π-electron would be wider than that of the nitryl group due to the introduced carbon-carbon double bond[31,32]. Therefore, the interactions between terminal acceptor and donor of the three molecules are different, which is expected to achieve different memory device characteristics. Herein, all the three molecules contain the same electron donor - bi-(n-butyl-carbazole) unit which has been widely applied in the organic photoelectric semiconductors devices for its high ionization potential and good molecular planarity[33,34]. The introduction of the bi-(n-butyl-carbazole) not only expands the electron delocalization to lower the energy gap but also enhances the molecular thermodynamics and the thin-film stability. The results showed that the memory devices based on **BCz-BT**, **BCz-NO_2** and **BCz-CN** three molecules exhibited volatile SRAM, nonvolatile WORM and nonvolatile rewritable flash characteristics, respectively. The in situ UV-vis absorption spectra of thin films at the ON and OFF states and quantum-chemical calculations were carried out to investigate the storage mechanism. We hope the tunable memory models through adjusting the terminal eletron-acceptors could give a guidance for rational memory materials design and synthesis in the future.

Experimental

Materials

Carbazole (95%), 2-amino-thiophenol (98%) and n-butyl bromide is purchased from Alfa Aesar. Iron trichloride, ammonium acetate, malononitrile, acetate acid, fuming nitric acid, phosphorus oxychloride, dimethylfomamide, dichloromethane, potassium carbonate, anhydrous sodium sulphate and other solvents were all purchased from Shanghai Chemi Reagent Co. Ltd. All solution and reactants were commercially available and used with no further purification.

Instruments

^{1}H NMR and ^{13}C NMR spectra were recorded on a Varian INOVA 400 MHz with DMSO-d_6 as the solvent and TMS as the internal standard. Thermal properties were estimated from a PE TGA-7 thermo-gravimetric analysis system (TGA) under a nitrogen atmosphere at a heating rate of 20 C min^{-1}. UV–vis absorption spectra were recorded by a Shimadzu UV 3500 spectrophotometer at room temperature. Cyclic voltammetry (CV) was performed at room temperature using a CorrTest CS Electrochemical Workstation analyzer. SEM images were taken on a Hitachi S-4700 scanning electron microscope. The surface morphology of the films is examined by atomic force microscopy (AFM) using an SPA 400 system from Seiko Instruments Inc., Japan. The device fabrications were employed by Mini Spectros Deposition System (Kurt.J.Lesker, England). All electrical measurements of the device were at room temperature under vacuum or nitrogen atmosphere conditions without any other encapsulation, using an Agilent Technologies B1500A semiconductor parameter analyzer.

Synthesis of compounds

9, 9'-dibutyl-9H, 9'H-3, 3'-bicarbazole **2** was synthesized according to literature[28]. Phosphorus oxychloride (2 mL, 21.8 mmol) was added drop wise to DMF (5 mL) at 0℃, and the mixture was stirred for 0.5h at this temperature. 9, 9'-dibutyl-9H, 9'H-3, 3'-bicarbazole (4.4 g, 10 mmol) was added and the reaction mixture was stirred at 75 ℃ for 5h (**Fig.1**). Then, the mixture was cooled to room temperature, poured into ice water and carefully neutralized with sodium hydroxide. The solution was extracted with dichloromethane (3*50 mL). The organic phase was washed with water and dried over anhydrous sodium sulphate. After filtration, the solvent was removed. The crude product was purified by silica gel column chromatography to give compound **3** (2.13 g, 45% as faint yellow powder. ^{1}H NMR (400 MHz, DMSO-d_6), δ (ppm): 0.86-0.92 (t, 6H), 1.32-1.38 (m, 4H), 1.79-1.85 (m, 4H) 4.53-4.59 (t, 4H), 7.28-7.31 (t, 1H), 7.60-7.62 (d, 2H), 7.55-7.57 (d, 2H), 7.80-7.82 (d, 1H), 7.86-7.89 (t, 2H), 8.07-8.09 (d, 1H), 8.37-8.40 (d, 1H), 8.58 (s, 1H), 9.29 (s, 1H).

Synthesis of 2-(9, 9'-dibutyl-9H, 9'H-3, 3'-bicarbazol-6-yl) benzo[d]thiazole (4, BCZ-BT) This compound had been reported by our cooperative group[28]. A mixture of the compound **3** (1 g, 2 mmol), 2-aminothiophenol (0.25g, 2 mmol), and DMSO (40 mL) was heated in an oil bath to a bath temperature of 160 C, held at that temperature for 4 h, and then poured into water. The separated solids were collected, dissolved in 1:4 acetic acid-water (50 mL), filtered, and washed with water and dilute sodium bicarbonate solution. These solids were recrystallized from ethanol to give compound **4** (0.9 g, 78%), faint yellow powder. ^{1}H NMR (400 MHz, $CDCl_3$), δ (ppm): 0.96-0.99 (t, 6H), 1.43-1.47 (m, 4H), 1.91-1.92(m, 4H), 4.37-4.39 (t, 4H), 7.37-7.54 (m, 7H), 7.83-7.93 (m, 3H), 8.08-8.23 (t, 3H), 8.54 (s, 1H), 8.4 4 (s, 1H), 8.89-9.01 (t, 2H). ^{13}C NMR (100 MHz, $CDCl_3$), δ (ppm): 14, 20.7, 31.5, 43.3, 109.1, 109.2, 109.5, 119.4, 120.7, 121.7, 122.8, 123.6, 123.7, 124.7, 124.8, 125.6, 126.3, 127.4, 128.7, 132.8, 133.1, 134.4, 135.1, 140.2, 140.3, 140.5, 142.7, 148.1, 154.6, 169.6.

Synthesis of 9, 9'-dibutyl-6-nitro-9H, 9'H-3, 3'-bicarbazole (5, BCZ-NO$_2$) Compound **2** (2.16 g, 4.8mmol) and fuming nitric acid (0.2 mL) were dissolved in 60 mL and 5 mL acetic acid respectively, fuming nitric acid solution was dropped into the reaction mixture very slowly for about 1 h, and the reaction mixture was stirred at room temperature for 2h. Then the mixture was poured into water, filtered, and the residue was washed with water. The crude product was purified by silica gel column chromatography to give **5** (1.5 g, 64% as yellow powder. ^{1}H NMR (400 MHz, DMSO-d_6), δ (ppm): 0.89-0.93 (t, 6H), 1.31-1.38 (m, 4 H), 1.78-1.82 (m, 4H), 4.42-4.46 (t, 3H), 4.54-4.57 (t, 3H), 7.21-7.25 (t, 1H), 7.27-7.31 (t, 1H), 7.48-7.52 (t, 2H), 7.59-7.66 (m, 2H), 7.70-7.74 (m, 3H), 7.79-7.81 (d, 1H), 8.02-8.04 (d, 1H), 8.20-8.1 (d, 1H), 8.25 (s, 1H). ^{13}C NMR (100 MHz, DMSO-d_6), δ (ppm): 14.2, 20.2, 31.1, 42.7, 109.9, 110.1, 110.9, 112.8, 117.8, 119.4, 120.4, 112.3, 122.9, 125.6, 126.3, 126.6, 127.6, 129.0, 139.9, 140.3, 140.9, 141.3, 143.0.

Synthesis of 2-((9, 9'-dibutyl-9H, 9'H-3, 3'-bicarbazol-6-yl) methylene) malononitrile (6, BCZ-CN) A mixture of the compound **3** (1 g, 2 mmol), malononitrile (0.3 g, excess) and ammonium acetate (<0.1 g, catalyst) dissolved in 40 mL methanol and the reaction mixture was stirred at room temperature for 4h. Then the mixture was poured into water, filtered and the residue was washed with water. The crude product was purified by silica gel column chromatography to give **6** (0.6 g, 58% as purplish red powder. ^{1}H NMR (400 MHz, DMSO-d_6), δ (ppm): 0.86-0.89 (t, 3H), 1.27-1.35 (m, 4H), 1.77-1.83 (m, 4H), 4.40-4.44 (t, 4H), 7.20-7.25 (t, 3H), 7.45-7.50 (t, 1H), 7.59-7.67 (m, 2H), 7.75-7.85 (m, 3H), 7.93-7.96 (d, 1H), 8.16-8.19 (d, 1H), 4.44-8.48 (t, 2H), 8.55 (s, 1H), 8.78 (s, 1H). ^{13}C NMR (100 MHz, DMSO-d_6), δ (ppm): 14.2, 20.2, 30.2, 42.6, 75.1, 109.8, 110.1, 111.0, 115.1, 115.9, 119.0, 119.2, 121.0, 122.7, 123.1, 123.2, 125.5, 126.3, 126.5, 127.0, 127.9, 132.1, 134.9, 139.8, 140.2, 141.0, 144.2, 161.8.

Fabrication of memory devices

The memory devices were fabricated by the sandwiching the **BCZ-BT**, **BCz-NO$_2$** and **BCz-CN** active layer between the indium-tin-oxide (ITO) bottom electrode and the Al electrodes. The ITO glass was cleaned with putty-powder; and then ultrasonic cleaning in deionized water, acetone and absolute ethyl alcohol solution successively was used to obtain a cleaner surface. The following operations are carried out in a glove box

with oxygen-content and water-content below 1 ppm. The compounds were deposited on ITO electrode with a 2 Å s^{-1} deposition rate under the vacuum of $8*10^{-7}$ Torr. Then a layer of Al was thermally evaporated and deposited onto the active films surface at about $1*10^{-6}$ Torr through a shadow mask to form the top electrode so as to define an active cross area of 0.0314mm^2 (a nummular point with a radius of 0.1mm).

Results and discussion

Characterization of the Compounds

The chemical structures and synthetic routines are shown in Fig. 1, and their structures identified by the 1H NMR and 13C NMR (Fig S1).

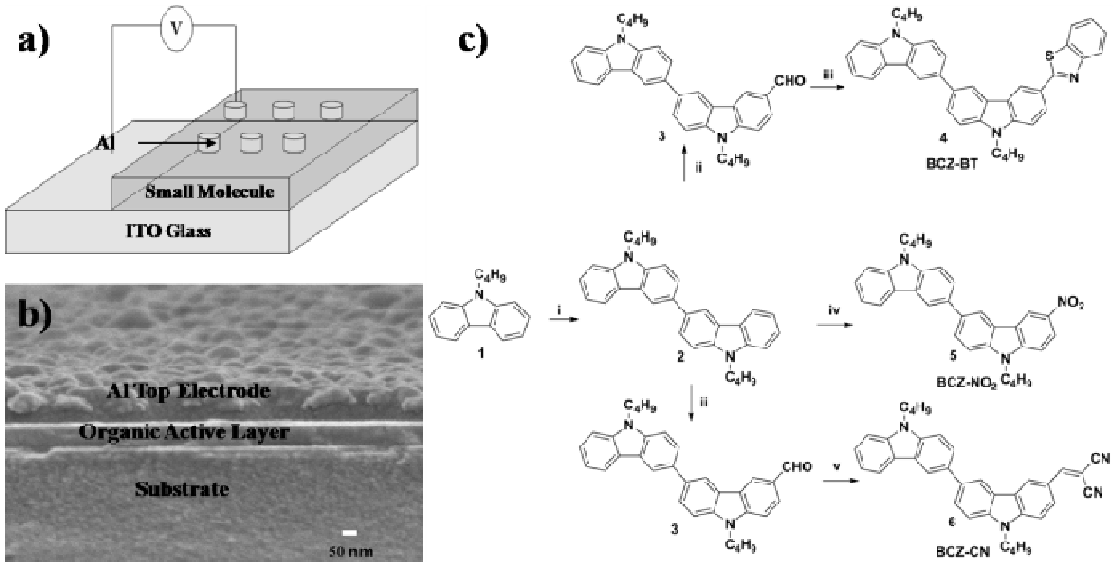

Fig.1 a), Schematic diagram of sandwich device based on the **BCZ-BT**, **BCZ-NO_2** and **BCZ-CN**, **b**), SEM image of the cross section of a memory cell, **c**), Synthetic routines of the BCZ derivatives. Reagents and conditions: (i) $FeCl_3/CH_2Cl_2$; (ii) $POCl_3$, DMF; (iii) o-amino thiophenol, ammonium acetate; (iv) fuming HNO_3, AcOH; (v) malononitrile, ammonium acetate.

The thermo gravimetric analysis (TGA) curves of **BCZ-BT**, **BCZ-NO_2**, and **BCZ-CN** with a high T_d value 344□, 314℃, 292℃, respectively (**Fig S2**). This ensures the molecules structure would not be decomposed during thermal vacuum evaporation process or the local area joule heat raised from the course of device operation, in other words, the synthesized molecules can be used in long-term thermally stable memory devices.

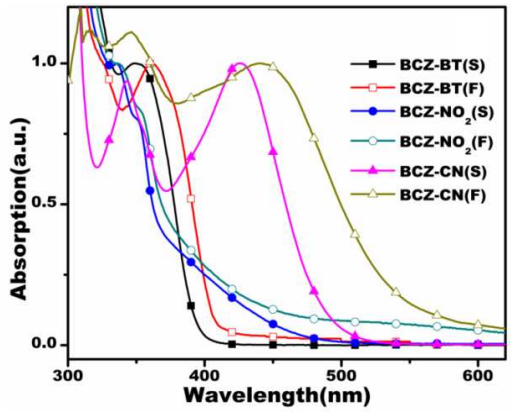

Fig.2 The UV-vis absorption spectra of compounds (**BCZ-BT**, **BCZ-NO_2** and **BCZ-CN)** in $1x10^{-5}$mol L^{-1} in CH_2Cl_2 solution and films of quartz glass substrate

Fig. 2 shows the optical absorption spectra of the **BCZ-BT**, **BCZ-NO_2** and **BCZ-CN** in dichloromethane solution and thin films. Obviously, the UV-vis spectra of **BCZ-CN** consisted of two absorption bands is observed, the high-energy absorption bands (around 345 nm) can be attributed to the π–π* transition, mainly arising from the bi-carbazole-vinyl moieties. The low-energy absorption bands (around 430nm) can be assigned to the intramolecular charge transfer (ICT) between the donor and acceptor moieties of the **BCZ-CN**. The red-shift of maximum absorption wavelength from high-energy absorption to the low-energy absorption band gets up to 90 nm, which indicates intensive intramolecular interaction between the bicarbazole and dicyanovinyl moiety. However, the low-energy absorption bands are not observed from the **BCZ-BT** and **BCZ-NO_2** absorption curves, indicating the CT complex is not formed in the ground state. And the absorption wavelength maximum arising from the π–π* transition are about 360 nm and 335 nm, respectively. From the absorption peaks of π–π* transition, it could be inferred that electron-delocalized extent of π-electron is followed **BCZ-BT>BCZ-CN>BCZ-NO_2**. Compared with absorption spectra in solution, a red-shift about 20nm, 10nm and 50 nm respectively for **BCZ-BT**, **BCZ-NO_2**, and **BCZ-CN** are observed in films. In addition, the CT transition of **BCZ-CN** in solid state shows a more obvious red-shift compared with that of the solution state. This red-shift might be related to the formation of molecular head-to-tail aggregates and/or increased polarity in the thin film[35]. The absorption onset of the thin-films correspondingly red-shifted from ~410 nm in **BCZ-BT** to ~400 nm in **BCZ- NO_2** and to ~550 nm in **BCZ -CN**, implying a reduction in the optical band gap of the D–A molecules with strengthening the interaction between the donor and the acceptor. The Eg values of the three compounds from the absorption onsets of the films are estimated

to be 3.03 eV, 3.13 eV and 2.28 eV, respectively. The detailed experimental data are summarized in **Table 1**.

Table 1 Thermal, optical, and electrochemical properties of the prepared D–A compounds

Compound	T_d/℃	λmax/nm	[a]Eg/eV	[b]Eox/eV	HOMO/eV	LUMO/eV
BCZ-BT	344	334	3.03	0.91	-5.23	-2.2
BCZ-NO_2	314	361	3.13	1.18	-5.54	-2.41
BCZ-CN	292	344/426	2.28	0.94	-5.32	-3.04

[a] The data were calculated using the following equation: Eg=1240/λonset of the films absorption spectra, [b] The HOMO energy levels were calculated from cyclic voltammetry with reference to ferrocene.

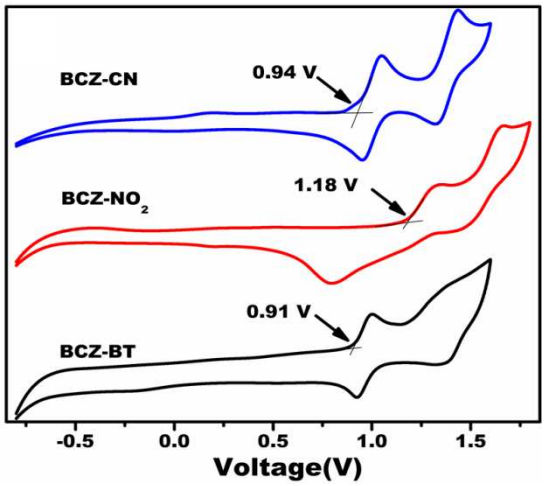

Fig.3 Cyclic voltammograms of **BCZ-BT**, **BCZ-NO_2** and **BCZ-CN** solution (10^{-3}mol/L, CH_2Cl_2) at 10mVs^{-1} scan rate.

The electrochemical properties of these molecules investigated by cyclic voltammetry (CV) in 0.1 mol·L^{-1} tetrabutylammonium hexafluorophosphate dichloromethane solution; platinum disk electrode, Ag/AgCl and platinum disk electrode were used as the working electrode, reference electrode and counter electrode respectively. The cyclic voltammograms are depicted in **Fig.3**. A couple of reversible oxidation peaks are obvious observed for all molecules which could be attributed to bicarbazole moieties. The primary onset oxidation potential (E_{Ox}) vs. Ag/AgCl reference electrode are 0.91 V for **BCZ-BT**, 1.18 V for **BCZ-NO_2** and 0.94 V for **BCZ -CN**, respectively. The corresponding standard oxidation potential of the external ferrocene/ferrocenium (Fc/Fc^{2+}) was measured to be 0.48 V, 0.44 V and 0.42 V vs. Ag/AgCl, respectively. The highest occupied molecular orbital (HOMO) energy levels of the D-A molecules are determined to be -5.23 eV, -5.54 eV and -5.32 eV, respectively (HOMO =-[E_{Ox} (onset) +4.8-E_{Fc}] eV). Thus, the lowest unoccupied molecular orbital (LUMO) energy levels are estimated to be -2.2 eV, -2.41 eV and -3.04 eV, respectively (LUMO = [HOMO + E_g (band gap)] eV). Herein, BCz-NO_2 reveals lower HOMO level but higher LUMO level, compared to those of BCz-CN, which is relative to the molecular conjugated degree and the interaction between the electron donor and acceptor. It is well known that the donor groups would increase the HOMO level and the acceptor would decrease the LUMO level in a D-π-A framework. To the **BCz-NO_2**, it is a D-A framework structure, namely there is no π-conjugate linkage between the donor and the acceptor. Besides, the interaction between BCz and NO_2 is p-π conjugation. To the **BCz-CN**, the interaction between donor and acceptor is π-π conjugation and the introduced π-conjugate linkage-vinyl group expands the electronic delocalized extent. So the conjugate degree of the **BCz-NO_2** is lower than the **BCz-CN**, the corresponding energy gap of BCz-NO_2 and BCz-CN are 3.03 eV and 2.28 eV, respectively. Namely **BCz-NO_2** reveals lower HOMO level but higher LUMO level. The work functions of cathode (Al electrode) and anode (ITO glass) are 4.2 eV and 4.8 eV, respectively. The energy barriers between the cathode and organic semiconductors are 2.0 eV, 1.79 eV and 1.16 eV for **BCZ-BT**, **BCZ-NO_2** and **BCZ-CN**, respectively. While the energy barriers between the anode and organic semiconductors are 0.43 eV, 0.74 eV and 0.52 eV. Therefore, these D-A molecules could be treated as p-type semiconductors.

The thin film morphologies of three small-molecules implemented by atomic force microscopy (AFM) were shown in **Fig.4**. The surface morphologies of three molecules all present uniform grain-like and smooth interface. The surface root-mean-square roughness (RMS) of thin films are 2 nm for **BCZ-BT**, 3.4 nm for **BCZ-NO_2** and 6.2 nm for **BCZ-CN**, respectively, indicating a favorable and stable interfacial contact with electrodes, which could effectively prevent Al nanoparticles from diffusion into films during the Al electrode deposition process.

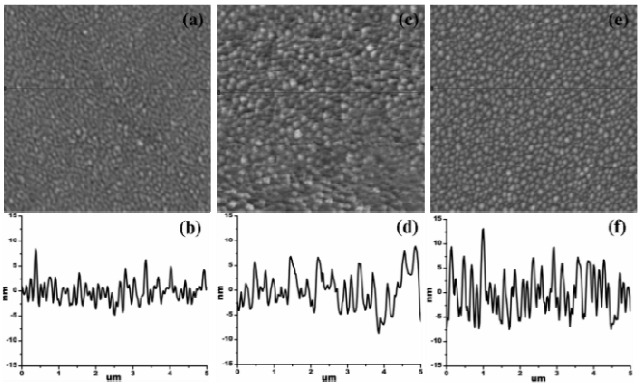

Fig.4 Tapping-mode (5μ m × 5μ m) AFM topography (**a**, **c**, **e**) of **BCZ-BT**, **BCZ-NO_2** and **BCZ-CN** films on ITO substrates and corresponding typical cross-section profile images (**b**, **d**, **f**)

Electrical characterization

Fig.1 (a) shows the schematic diagram of the indium-tin oxide/**BCZ-BT** or **BCZ-NO_2** or **BCZ-CN**/aluminum device. Estimated by the scanning electronic microscopic (SEM) image of the cross section of a storage cell， the thickness of the intermediate organic layer is about 70 nm (**Fig.1** (**b**)) and the thickness of top Al electrode is about 100 nm.

The electrical properties of the devices were measured at room temperature under ambient conditions without any encapsulation. **Fig.5** shows the current–voltage (I–V) curves of the ITO/ **BCZ-BT**, **BCZ-NO$_2$**, and **BCZ-CN** /Al electrode sandwiched devices, respectively. The current-voltage (I/V) characteristic of **BCZ-BT** based device in **Fig.5 (a)** exhibited two remarkable conductivity states. In the first voltage scan from 0 to -4 V, an abrupt increase in current from 10^{-6} A to 10^{-2} A was observed with a low switching threshold voltage about 1.6 V (onset), corresponding to the transition from low-conductivity state (OFF state) to high-conductivity state (ON state). This electrical transition served as the "writing" process for the memory device. Then a same direction and reversed scan voltage were applied sequential (sweep 2 and sweep 3), and the device remained in its high-conductivity state. About five minutes later, the device could be switched renewably from original OFF state to high-conductivity state (sweep 4). Namely, a refresh voltage is required to maintain the high-conductivity state (i.e., the written data), or the device would revert from the high-conductivity state to the initial low-conductivity state after several minutes, which was typical characteristic of the volatile static random access memory (SRAM). In addition, the ON/OFF ratio was about 10^4 which promised a low misreading rate for the device.

The device based on compound **BCZ-NO$_2$** showed distinct bi-electrical stable states with the threshold voltage about 1.8 V and the ON/OFF current ratio about 10^3, as shown in the **Fig.5 (b)**. The device underwent a transition from the low-conductivity state (OFF state) to the high-conductivity state (ON state) when the applied negative voltage reached the threshold. When a repeated negative voltage (same direction) sweep or the reverse voltage sweep was operated, it did not return to the original OFF state even after long time. Namely it exhibited the non-volatile write once read many times (WORM) characteristic.

The memory effect of **BCZ-CN** showed in **Fig.5 (c)**. It was obvious that a sharp increase in current occurred at about - 1.5 V (sweep 1), indicating the device switched to a high-conductance state (ON state). And the memory device remained in the ON state during the second sweep from 0 to -4 V (sweep 2). This OFF to ON conversion could be viewed as a ''writing'' process in a digital-memory cell. The ON state could be returned to the OFF state when the reversed positive voltage approached around 3.5 V (sweep 3). The OFF state could be switched back to the low-resistance state by applying a negative bias again (sweep 5), resulting in a repeated OFF state to ON state. This phenomenon suggested that the **BCZ-CN** based memory device exhibited non-volatile rewritable flash memory characteristic. The maximum ON/OFF ratio was about 10^4, indicating high-resolution and low-error-rate data storage for the memory device.

From Fig. 5, we can concluded that the switch-on voltages of the BCz-BT, BCz-NO2 and BCz-CN are -1.5 V, -2.0 V and -1.6 V, respectively, which are well consisted with the energy barriers between the anode and organic semiconductors' HOMO levels discussed in former part. All the devices based on three molecules showed good stability under a constant stress or continuous read pulses voltage of −1.0V on the low-conductivity and high-conductivity states (**Fig.S3**).

The memory device based on BCz molecule exhibited the more volatile characteristic, which could be switched on repeatable with 1-2 min interval (**Fig.S4**), which is shorter than that of **BCZ-BT** about 5 min. This illustrated that the volatile time is relative to the electron acceptor ability, as the electron acceptor becomes weaker, the volatile time is shorter[15].

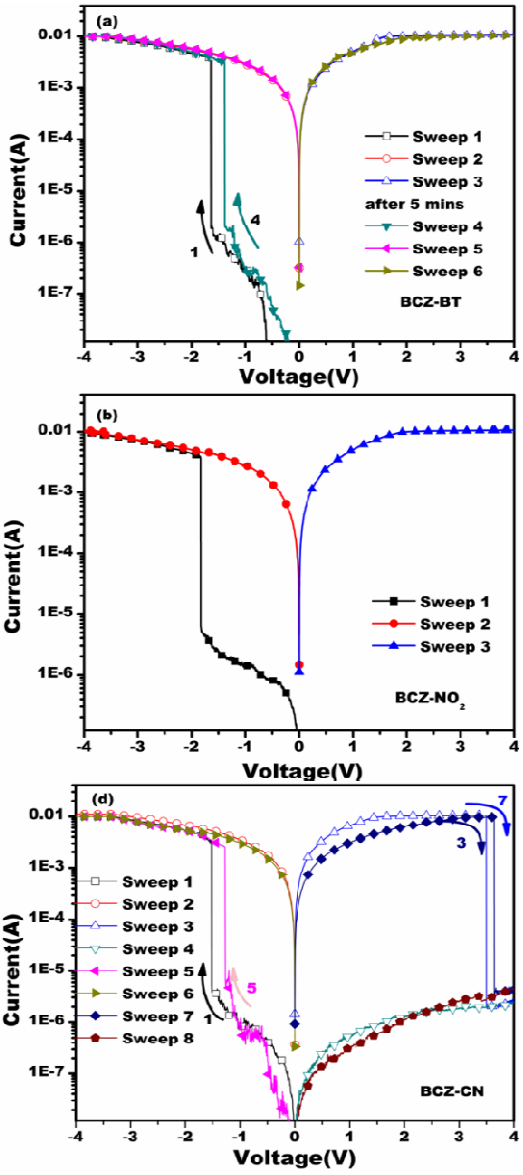

Fig.5 (**a**, **b**, **c**) Current–voltage (I–V) characteristics of the memory devices based on **BCZ-BT**, **BCZ-NO$_2$**, and **BCZ-CN**.

Memory Mechanism Discussion

According to the related reported literatures, the switch mechanisms of charge trapping and charge transfer complex were proposed to discuss the switch model of **BCz-BT**, **BCz-NO$_2$** and **BCz-CN**, respectively. First of all, charge transport mechanism of the OFF and ON states were investigated according to various current theoretical models, The experimental data can be fitted pretty well according to proper theoretical model, as shown in **Fig.4S**. The OFF states for the ITO/ **BCz-BT**, **BCz-NO$_2$** and **BCz-CN** /Al devices can be elucidated as ohmic current model (the voltage below -0.8 V) and space-charge-limited-current model (SCLC, voltage from threshold voltage). When under a

low negative bias, the *I-V* curves are linear and can be fitted by the ohmic conductance model (I∝V). In this stage, the current is very low (about 10^{-6} A) and the active layer can be treated with insulators. With the continuous increasing of the bias (-0.8 to threshold voltage V), Schottky barriers (greater than 0.4 eV) are formed for these devices. The hole injection from the ITO glass would be easier than the electron injection from Al electrode due to the low hole injection energy barriers. Thus, when the exerted bias exceeds the Schottky barriers, holes begin to inject and accumulate gradually near the anode, then the space-charge-limited-current is formed and the *I-V* curves follow $I \propto V^2$ relationship, indicating that the conductance mechanism is dominated by SCLC model in this stage and the traps of thin films were filled with the injected charge. Then, the current increased suddenly to switch the device from the high-resistance states to the low-resistance states. For the ON states (>threshold voltage), the *I–V* curve characteristics are dominated by Ohmic current model again [36,37] (**Fig. S5**).

In order to make the proposed switch mechanisms more convincing and to better understand the effect of terminal acceptors on the storage type transformations, molecular simulation and in situ UV-vis absorption spectra of ON/OFF state thin films were carried out. The quantum chemical calculations were performed using density functional theory (DFT) method of B3LYP with 6-31G basis set. The highest occupied molecular orbital (HOMO) and the lowest unoccupied molecular orbital (LUMO) surfaces of the **BCz-BT**, **BCz-NO$_2$** and **BCz-CN** are shown in **Fig.6**. It can be observed clearly that all the D-A molecular HOMO surfaces obtained are evenly delocalized on the electron donor moiety (bicarbazole). The LUMO surfaces of **BCz-BT** and **BCz-CN** are delocalized on the terminal acceptors and adjacent carbazole moiety, but **BCz-NO$_2$** preferred to localize on nitryl and adjacent benzene ring side. The simulate HOMO–LUMO gap was 3.14 eV, 3.01eV and 2.55 eV for **BCz-BT**, **BCz-NO$_2$** and **BCz-CN**, respectively, in which the band gap of **BCz-CN** is smallest and will be favorable for the HOMO interacting with the LUMO to form charge transfer complex[35], this simulation result is consisted with the former UV-vis results.

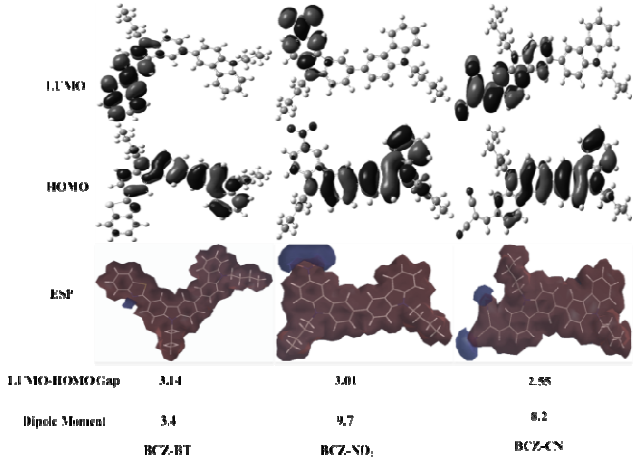

Fig.6 HOMO and LUMO surfaces, electrostatic potential (ESP), bandgap and dipole moment of **BCz-BT**, **BCz-NO$_2$** and **BCz-CN** obtained by simulation based on their optimized ground-state structures.

The in situ UV-vis absorption spectra of ON state thin films showed that CT absorption bands were not occurred, which indicated that the charge transfer complexes did not form for **BCz-BT** and **BCz-NO$_2$** even when an external electric field was exerted (**Fig 7**) [38]. It implied that trapping electron governed the switching behaviors of the **BCz-BT** and **BCz-NO$_2$** based memory devices. Namely, the electron-deficient groups of benzothiazole and nitryl were employed as the electron trapping sites[39,40]. The electron affinity (depth of electron trapping sites) could be visually depicted by the negative ESP regions (blue color), showed in **Fig. 6**, from which we could deduce the thiazole is a weak electron trap and nitryl is a strong electron trap according to the blue area. Owing to the weak electron affinity and polarization effect in BCZ-BT molecule, it was hard for the exciton (electron-trapped molecule) to maintain in the high-energy state when the external electric field was removed. Thus, the **BCz-BT** based device exhibited volatile SRAM memory behavior. In contrast, the nitryl is strong electron-withdrawing group and the simulate dipole moment is up to 9.7 D, indicating that the trapped-electron could be maintained in a long time even though the applied bias was removed[29]. Thus, the **BCz-NO$_2$** based device showed stable non-volatile WORM memory characteristic. The deductive memory mechanism could be confirmed by the in situ UV-vis absorption spectra of ON/OFF state thin films (**Fig.7 a, b**). Five minutes later, the ON/OFF state UV-vis absorption curves of **BCz-BT** were almost coincided. On the contrary, an obviously decreased absorption intensity of the ON state relative to the original state was found to **BCz-NO$_2$**. The test results of in-situ UV-vis absorption spectra were different from the reported literatures that the absorption intensity of the ON state was increased [38,41]. We presumed that the absorption intensity was proportional to the concentration of the ground state molecule. Undergoing an exerted electric filed, part of molecules had been excited and the excited state was still remained when subsequently irradiating the on-switched thin film under UV-vis light, and thus the decreased absorption intensity was observed in the spectra. The results showed that memory transferred from ON state to OFF state to **BCz-BT** after five minutes, but the **BCz-NO$_2$** based device still was retained the ON state.

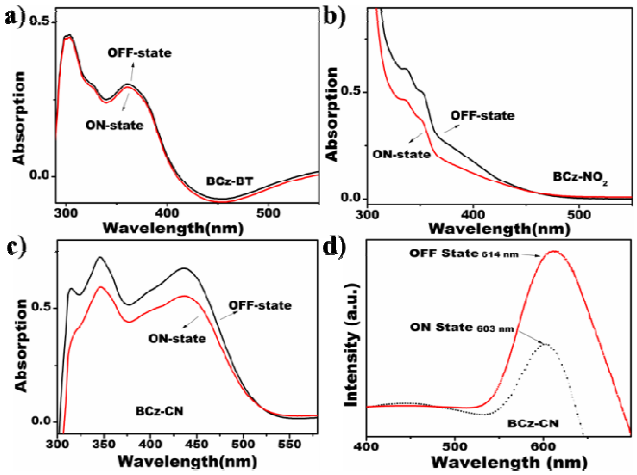

Fig.7 (a, b, c) The in-situ UV-vis spectra of ON/OFF state thin films to BCz-BT, BCz-NO2 and BCz-CN; (d) the in-situ photoluminescence spectrum of ON/OFF state thin films to compound BCz-CN (the test data without any normalization).

BCz-CN has a typical asymmetric D-π-A structure framework, with small energy gap and good molecular planarity, which will benefit the formation of intramolecular and/or intermolecular charge transfer complex in the solid state. In addition，cyano is an intense electron-withdrawing group like the nitryl group and the simulate dipole moment is up to 8.2 D. Thus, the formed charge-separated state is stable and could be maintained in a long time. Namely, the switched-on memory device is not return to its original OFF state when the applied voltage removes. For **BCz-CN**, the donor and acceptor are linked by vinyl bond which limits the free rotation of the two parts; besides, the carbazole is rigid planar unit, which could decrease degree of conformational freedom by charge transfer interaction, too. So, when an inverted positive voltage was exerted, the CT complex could be relaxed and the low-resistance state returned to the high-resistance state[23]. This switch behavior is consistent with the characteristic of rewritable flash memory. Obviously, the formed CT complex was not reflected by the in-situ UV-vis spectrum of the **BCz-CN**. To better confirm the exciplex formed under the bias voltage, fluorescence emission spectra of ON/OFF state thin films were measured to describe this process (**Fig.7 d**) [41]. It was obvious that intensity of the photoluminescence spectrum was quenched by two orders of magnitude, indicating that the CT complex was formed under an exerted bias, which further proved our proposed switch mechanism.

Conclusion

In this work, we illustrated the electronic effect of terminal acceptors on the memory properties and the interaction between donor and acceptor based on three donor-acceptor organic conjugated small-molecules **BCz-BT**, **BCz-NO$_2$** and **BCz-CN**. The as-fabricated devices based on **BCz-BT** showed volatile SRAM switch behaviour, while that based on **BCz-NO$_2$** and **BCz-CN** exhibited stable non-volatile WORM and flash memory characteristics, respectively. The results indicated that i) device based on the molecule with weak electronic effect between donor and acceptor (**BCz-BT**) induced volatile memory SRAM behaviour, ii) strong inductive effect but weak conjugative effect (**BCz-NO$_2$**) induced non-volatile WORM characteristic, iii) strong inductive effect and conjugative effect (**BCz-CN**) caused non-volatile flash switch behaviour which arises from the formation of CT complex. Overall, other relative studies are still in progress by our group and the present experimental results of this paper would provide new strategies to investigate the organic resistive memory devices.

Acknowledgements

This work was financially supported by the Chinese Natural Science Foundation (21176164, 21206102 and 21336005), the NSF of Jiangsu Province (BE2013052), a project of the Department of Education of Jiangsu Province (12KJB430011), Suzhou Nano-project (ZXG2012023) and Project supported by the Specialized Research Fund for the Doctoral Program of Higher Education of China (Grant No. 20113201130003 and 20123201120005).

Notes and references

[a] College of Chemistry, Chemical Engineering and Materials Science, Collaborative Innovation Center of Suzhou Nano Science and Technology, Soochow University, Suzhou 215123, China. Fax: +86 512 65880367; Tel: +86 512 65880368; E-mail: lujm@suda.edu.cn.

[b] State Key Laboratory of Treatments and Recycling for Organic Effluents by Adsorption in Petroleum and Chemical Industry, Suzhou 215123, P. R. China.

Electronic Supplementary Information (ESI) available: [^{1}H and ^{13}C NMR spectra of **BCz-NO$_2$** and **BCz-CN** (S1); Thermo-gravimetric analysis (TG A) curves (S2); Effect of retention time at 0.8 V on OFF and ON states of **BCz-BT**, **BCz-NO$_2$** and **BCZ-CN** under a constant stress of 0.8 V (S3); T he memory perfermance of the ITO/Bcz/Al (S4); Experimental and fitted data of I-V curves for the memory devices of the OFF and ON states for **BCz-BT**, **BCz-NO$_2$** and **BCZ-CN** (S5)]. See DOI: 10.1039/b000000x/

1 Q.-D. Ling, D.-J. Liaw, C. Zhu, D. S.-H. Chan, E.-T. Kang and K.-G. Neoh, *Prog. Polym. Sci.,* 2008, **33**, 917.
2 C.-L. Liu and W.-C. Chen, *Polym. Chem.,* 2011, **2**, 2169.
3 Y. Chen, B. Zhang, G. Liu, X. Zhuang and E. T. Kang, *Chem. Soc. Rev.,* 2012, **41**,4688.
4 T. Lee, Y. Chen, *Mater. Res. Soc. Bull.,* 2012, **1**, 144.
5 T. Kurosawa, T. Higashihara and M. Ueda, *Polym. Chem.,* 2013, **4**, 16.
6 B. Cho, S. Song, Y. Ji, T.-W. Kim and T. Lee, *Adv. Func. Mater.,* 2011, **21**, 2806.
7 F. Zhao, J. Liu,X. Huang, X. Zou, G. Lu, P. Sun, S. Wu, W. Ai, M. Yi, X. Qi,L. Xie, J. Wang, H. Zhang and W. Huang, *ACS Nano.*, 2012, **6**, 3027.
8 Z. Yin, Z. Zeng, J. Liu, Q. He, P. Chen, H. Zhang, *Small*., 2013, **5**, 727
9 Y.-K. Fang, C.-L. Liu, C. Li, C.-J. Lin, R. Mezzenga and W.-C. Chen, *Adv. Funct. Mater.*, 2010, **20**, 3012.
10 D. M. Kim, S. Park, T. J. Lee, S. G. Hahm, K. Kim, J. C. Kim, W. Kwon and M. Ree, *Langmuir.,* 2009, **25**, 11713.
11 S. J. Liu, Z. H. Lin, Q. Zhao, Y. Ma, H. F. Shi, M. D. Yi, Q. D. Ling, C.-X. Zhu, E. T. Kang, W. Huang, *Adv. Funct. Mater*., 2011, **21**, 979.
12 A. D. Yu, T. Kurosawa, Y. H. Chou, K. Aoyagi, Y. Shoji, T. Higashihara, M. Ueda, C. L. Liu and W. C. Chen, *ACS Appl. Mater. Interfaces*., 2013, **5**, 4921.
13 L.-H. Xie, Q.-D. Ling, X.-Y. Hou and W. Huang, *J. Am. Chem. Soc.,* 2008, **130**, 2120.
14 T.-W. Kim, S.-H. Oh, H. Choi, G. Wang, H. Hwang, D.-Y. Kim and T. Lee, *Appl. Phys. Lett.,* 2008, **92**, 253308.
15 S. G. Hahm, T. J. Lee, D. M. Kim, W. Kwon, Y.-G. Ko, T. Michinobu and M. Ree, *J. Phys. Chem. C*., 2011, **115**, 21954.
16 X. D. Zhuang, Y. Chen, G. Liu, P. P. Li, C. X. Zhu, E. T. Kang, K. G. Noeh, B. Zhang, J. H. Zhu and Y. X. Li, *Adv. Mater.,* 2010, **22**, 1731.
17 P. Y. Gu, F. Zhou, J.Gao, G. Li, C. Wang, Q. F. Xu, Q. C. Zhang, J. M. Lu, *J. Am. Chem. Soc.*, 2013, **135**, 14086.
18 Y. Shang, Y. Wen, S. Li, S. Du, X. He, L. Cai, Y. Li, L. Yang, H. Gao and Y. Song, *J. Am. Chem. Soc.,* 2007, **129**, 11674-11675.
19 H. Li, Q. F. Xu, N. J. Li, R. Sun, J. F. Ge, J. M. Lu, H. W. Gu and F. Yan, *J. Am. Chem. Soc.,* 2010, **132**, 5542.
20 Y.-C. Lai, T. Kurosawa, W.-C. Chen, *Chem. Asian. J.,* 2013, **7**, 1514.
21 T. Kurosawa, Y.-C. Lai, A.-D. Yu, H.-C. Wu, T. Higashihara, M. Ueda and W.-C. Chen, *J. Polym. Sci., Part A: Polym. Chem.*, 2013, **51**, 1348.
22 Y.-G. Ko, W. Kwon, H.-J. Yen, C.-W. Chang, D. M. Kim, K. Kim, S. G. Hahm, T. J. Lee, G.-S. Liou and M. Ree, *Macromolecules.*, 2012, **45**, 3749.
23 C. J. Chen, Y. C. Hu and G. S. Liou, *Chem. Commun.,* 2013, **49**, 2536
24 C. W. Chu, J. Ouyang, J. H. Tseng, Y. Yang, *Adv. Mater.*, 2005, **17**, 1440.
25 S. Ko, R. Mondal, C. Risko, J. K. Lee, S. Hong, M. D. McGehee, J.-L. Brédas, Z. N. Bao, *Macromolecules.,* 2010, **43**, 6685.
26 B. Carsten, J. M. Szarko, H. J. Son, W. Wang, L. Lu, F. He, B. S.; Lou, S. J. Rolczynski, L. X. Chen, L. P. Yu, *J. Am. Chem. Soc.,* 2011, **133**, 20468.

27 X.-D. Zhuang, Y. Chen, B.-X. Li, D.-G. Ma, B. Zhang, Y. Li, *Chem. Mater*., 2010, **22**, 4455-4461
28 H. Y. Wang, G. Chen, X. Xu, H. Chen, S. J. Ji, *Dyes. Pigments.,* 2010, **86**, 238.
29 S. L. Lim, N.-J. Li, J.-M. Lu, Q.-D. Ling, C. X. Zhu, E.-T. Kang and K. G. Neoh, *ACS Appl. Mater. Interfaces*., 2008, **1**, 60-71.
30 S. Miao, Y. Zhu, H. Zhuang, X. Xu, H. Li, R. Sun, N. Li, S. Ji and J. Lu, *J. Mater. Chem. C.,* 2013, **1**, 2320.
31 Y. Shang, Y. Wen, S. Li, S. Du, X. He, L. Cai, Y. Li, L. Yang, H. Gao, Y. Song, *J. Am. Chem. Soc.,* 2007, **129**, 11674.
32 Y. Le, K. Nishida, M. Karakawa, H. Tada, Y. Aso, *J. Org. Chem.,* 2011, **76**, 6604.
33 S. G. Hahm, N.-G. Kang, W. S. Kwon, K. T. Kim. Y.-K. Ko, S. Y. Ahn, B.-G. Kang, T. H. Chang, J.-S. Lee, M. H. Ree, *Adv. Mater.,* 2012, **24**, 1062.
34 J. Lin and D. Ma, *Appl. Phys. Lett.,* 2008, **93**, 93505.
35 Y. Ma, X. Cao, G. Li, Y. Wen, Y. Yang, J. Wang, S. Du, L. Yang, H. Gao and Y. Song, *Adv. Func. Mater.,* 2010, **20**, 803.
36 Q.-D. Ling, Y. Song, S.-L. Lim, E. Y.-H. Teo, Y.-P. Tan, C. Zhu, D. S. H. Chan, D.-L. Kwong, E.-T. Kang and K.-G. Neoh, *Angew. Chem. Int. Ed.*, 2006, **45**, 2947.
37 H. Li, N. Li, R. Sun, H. Gu, J. Ge, J. Lu, Q. Xu, X. Xia and L. Wang, *J. Phys. Chem. C*., 2011, **115**, 8288.
38 C.-J. Chen, H.-J. Yen, Y.-C. Hu and G.-S. Liou, *J. Mater. Chem. C.,* 2013, **1**, 7623.
39 W. S. Kwon, B. C. Ahn, D. M, Kim, Y-G. Ko, S. G. Hahm, Y. K. Kim, H. J. Kim, M. H. Ree, *J. Phys. Chem. C*., 2011, **115**,19355.
40 Y.-K. Fang, C.-L. Liu, W.-C. Chen, *J. Mater. Chem.,* 2011, **21**,4778.
41 Y.-L. Liu, K.-L. Wang, G.-S. Huang, C.-X. Zhu, E.-S. Tok, K.-G. Neoh, E.-T. Kang, *Chem. Mater*., 2009, **21**, 3391.